



## Desorption dynamics of deuterium in CuCrZr alloy



Lan Anh Thi Nguyen <sup>a</sup>, Sanghwa Lee <sup>a</sup>, S.J. Noh <sup>b</sup>, S.K. Lee <sup>c</sup>, M.C. Park <sup>d</sup>, Wataru Shu <sup>e</sup>,  
Spencer Pitcher <sup>f</sup>, David Torcy <sup>f</sup>, David Guillermain <sup>f</sup>, Jaeyong Kim <sup>a,\*</sup>

<sup>a</sup> Department of Physics, HYU-HPSTAR-CIS High Pressure Reserach Center, Hanyang University, Seoul, 04763, South Korea

<sup>b</sup> Department of Physics, Dankook University, Cheonan-si, Chungnam, 31116, South Korea

<sup>c</sup> Nuclear Fusion Engineering Development Division, Korea Atomic Energy Research Institute, Daejeon, 34057, South Korea

<sup>d</sup> Material PIE and Rad-waste Disposal Division, Korea Atomic Energy Research Institute, Daejeon, 34057, South Korea

<sup>e</sup> Tritium Plant Section, ITER Organization, Route de Vinon-sur-Verdon, CS 90046-13067 St., Paul-lez-Durance, France

<sup>f</sup> Remote Handling and Radioactive Materials Division, ITER Organization, Route de Vinon-sur-Verdon, CS 90046-13067 St., Paul-lez-Durance, France

HPSTAR  
474-2017

### HIGHLIGHTS

- Desorption behavior of deuterium in CuCrZr alloys was investigated following the ITER scopes.
- Deuterium was embedded in CuCrZr alloys at a depth of less than 15  $\mu\text{m}$ , and can be completely retrieved in 15 min through dynamic pumping at 800 °C.
- Desorption rate of deuterium was inversely proportional to the increment of the thickness of the sample but proportional to the loading temperature.
- The trapping energies of deuterium in CuCrZr alloys were 62 and 79 kJ/mol.

### ARTICLE INFO

#### Article history:

Received 13 May 2017

Received in revised form

29 July 2017

Accepted 10 September 2017

Available online 12 September 2017

#### Keywords:

CuCrZr

Hydrogen isotope

Deuterium

Trapping energy

SIMS

### ABSTRACT

Desorption behavior of deuterium ( $\text{D}_2$ ) in CuCrZr alloy was investigated considering sample thickness, loading and baking temperature of deuterium followed by the ITER scopes. Cylindrical specimens of 1, 3, 5 mm thick with 4 mm diameter were exposed to deuterium at a pressure of 25 bar at 120, 240 and 350 °C for 24 h, then baked at 800 °C in a vacuum chamber maintained at a pressure lower than  $10^{-7}$  Torr. Deuterium desorption characteristics such as desorption rate and amount of deuterium in the sample were estimated by analyzing the desorption peaks monitored with a residual gas analyzer (RGA), and the trapping energy of deuterium was calculated using thermal desorption spectroscopy (TDS). Secondary ion mass spectroscopy (SIMS) results showed that deuterium atoms embedded in the sample at a depth of less than 15  $\mu\text{m}$  and desorbed as low as 400 °C. All absorbed deuterium atoms in the specimen were completely retrieved by dynamic pumping at 800 °C in 15 min. The desorption rate of deuterium per unit area was inversely proportional to the increment of the thickness of the sample, and was proportional to the loading temperature. Based on the assumption that a uniform distribution of interstitial sites for deuterium follows the Femi-Dirac statistics, the result of TDS demonstrated that the CuCrZr alloy has two types of trapping energies, which were estimated to be 62 and 79 kJ/mol.

© 2017 Elsevier B.V. All rights reserved.

### 1. Introduction

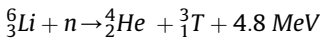
CuCrZr alloys are considered to be attractive structural materials for plasma-facing components (PFC) in fusion reactors, including in the International Thermonuclear Experimental Reactor (ITER), Demonstration Power Station (DEMO), Tore Supra (TS), and Joint

European Torus (JET) [1–3], because of their high thermal conductivity and stability at elevated temperatures, high fracture toughness and high resistance to radiation damage during plasma operation [4–7]. Furthermore, the materials also show excellent welding properties and good thermo-physical and mechanical behaviors, making them promising candidates for various purpose fusion devices [8]. Of these, precipitation hardened (PH) copper alloy, called PH-CuCrZr, has been used as a heat sink for first walls, diverters, heating systems, and in electrical strips or even as plasma facing materials [9].

\* Corresponding author.

E-mail address: [kimjy@hanyang.ac.kr](mailto:kimjy@hanyang.ac.kr) (J. Kim).

During the fusion reaction, tritium is produced when neutrons interact with lithium contained in the blanket wall of the tokamak. The reaction releases an exothermal energy of 4.8 MeV, and the tritium that is produced is retained in fusion reactors by permeation or transmutation. The production of tritium can be represented through the following process:



In general, hydrogen isotopes dissolve in interstitials or in lattice sites of the material and are retained by imperfect sites such as vacancies, grain boundaries, and impurities. Hydrogen retention will affect transport and the physical and mechanical properties of the host materials. The permeation of hydrogen and its isotopes through various materials such as tungsten, beryllium, stainless steel, and their alloys has been a focus of attention owing to its importance from both a scientific and an engineering perspective [10–13]. For example, the permeation of hydrogen isotopes through metals induces embrittlement and degradations such as lower tensile ductility or radiation hardening, due to the damaging effect on the structure and phase instabilities of the materials [14–18]. Thus, the permeation of hydrogen isotopes through materials is an important issue in the technical design of nuclear fusion devices. Tritium is of particular concern because it is radioactive, and its high permeability will result in unacceptably high rates of discharge to the environment. Yet despite the importance of the retention of hydrogen isotopes during the plasma operation, very limited studies of desorption behaviors of hydrogen isotopes in CuCrZr alloys have been reported, and it is thus necessary to quantify the desorption parameters to retrieve the embedded hydrogen isotopes for the safe storage and disposal of tritiated waste. Taking the example of deuterium, the ratio of deuterium to atoms on the surface of W,  $n_D/n_W$ , is 42 at. %, and the dissolved deuterium permeates into the structural components and affects not only the stability of devices and recycling to plasma, but also has an influence on the environmental safety [19]. While the transport properties including the permeability, diffusivity, and solubility of hydrogen isotopes in CuCrZr alloys have been scarcely studied [20–22], desorption parameters associated with uptake and retention of the isotopes in these alloys are not yet available.

For this reason, it is important to investigate the amount of absorbed hydrogen isotopes in CuCrZr alloys during the plasma operation and qualify desorption parameters in order to retrieve the embedded hydrogen isotopes for the safe generation of plasma. The mission of this study is to measure the deuterium removal efficiency from CuCrZr specimens scaled-down to the ITER scope for radwaste treatment and processing, and to estimate the desorption rates of deuterium in the samples.

## 2. Experimental procedure

CuCrZr alloys (grade ELBRODUR<sup>®</sup>G) were purchased from KME, Germany AG and Co., KG. The chemical compositions and physical

properties of CuCrZr alloy are shown in Table 1. To meet the ITER scope, a chunk of CuCrZr alloy was machine processed into several pieces having a rod shape with a thickness of 1, 3, and 5 mm and a diameter of 4 mm.

The surfaces of the samples were first mechanically polished using sandpaper (No. 100,000) followed by abrasive powder having an average particle size of 1  $\mu\text{m}$ . Polished samples were subsequently cleaned with methanol in an ultrasonic bath for 10 min. The surface roughness and structure of samples were analyzed using scanning electron microscopy (SEM), atomic force microscopy (AFM), Auger electron spectroscopy (AES) and X-ray diffraction (XRD) measurements.

Deuterium was loaded into samples using a laboratory-built system. The system is composed of two parts: 1) the gas delivery part formed with a D<sub>2</sub> cylinder, standard volume cell, and pressure gauges connected with 1/4" stainless steel tubes, and 2) a sample chamber connected with the gas delivery part using a VCR metal gasket, and 3) a pumping system which can evacuate the system to  $\sim 10^{-3}$  Torr. Samples were exposed to 25 bar of deuterium pressure at 120, 240 and 350 °C for 24 h.

Deuterium exposed samples were heated in a vacuum by using a baking system which was custom built based on the concept of a continuous flow system. The actual temperature of the sample was independently controlled and recorded from the temperature controller by using a K-type thermocouple placed near the sample. The out-gassed elements were identified, and the amount of partial pressure of desorbed deuterium was monitored over time using an RGA equipped with a quadrupole mass spectrometer. The partial pressure of the desorbed deuterium was integrated to estimate the amount of the element in the sample. The specimens were baked at 800 °C using a thermal heater at heating rates of 3.6–4.2 °C/sec from room temperature. 240 °C loaded 5 mm thick samples were baked at three different temperatures; 400, 600 and 800 °C.

A thermal desorption spectroscopy (TDS) system was built and data were analyzed to estimate the amount of desorbed elements and to determine the trapping energy of deuterium [23–26]. The samples were heated to 900 °C from room temperature at various heating rates ranging from 10 to 30 °C/min, and the desorption energy of deuterium was estimated by employing an Arrhenius equation.

## 3. Results and discussion

The morphology, roughness and the structure of the samples were determined by analyzing SEM, AFM and XRD data. Before the mechanical polishing, the color of the samples was dark-gray, suggesting that a natural oxygen layer with unknown organics covered the sample (see Fig. 1(a)). However, after the polishing, the samples showed a shiny surface with a traditional copper color, suggesting that most of the organic impurities and morphological surface defects had been removed (see Fig. 1(c)). The AFM images, as shown in Fig. 1 (b) and (d), are evidence that the surface roughness was significantly decreased from 80 to

**Table 1**  
Physical properties and chemical compositions of ELBRODUR<sup>®</sup>G alloy.

Density at 20 °C	8.9 g/cm <sup>3</sup>
Melting temp. (liquid)	1075 °C
Mean coeff. of linear thermal expan. (20–300 °C)	$18 \times 10^{-6}/\text{K}$
Modulus of elasticity	128 (GPa)
Thermal conductivity at 20 °C	330 W/(m·K)
Electrical conductivity	$48 \times 10^6$ (S/m)
Softening temperature	475 °C
Recrystallization temperature	700 °C
Composition	Cr:0.65, Zr:0.1 wt. %, Cu rem.

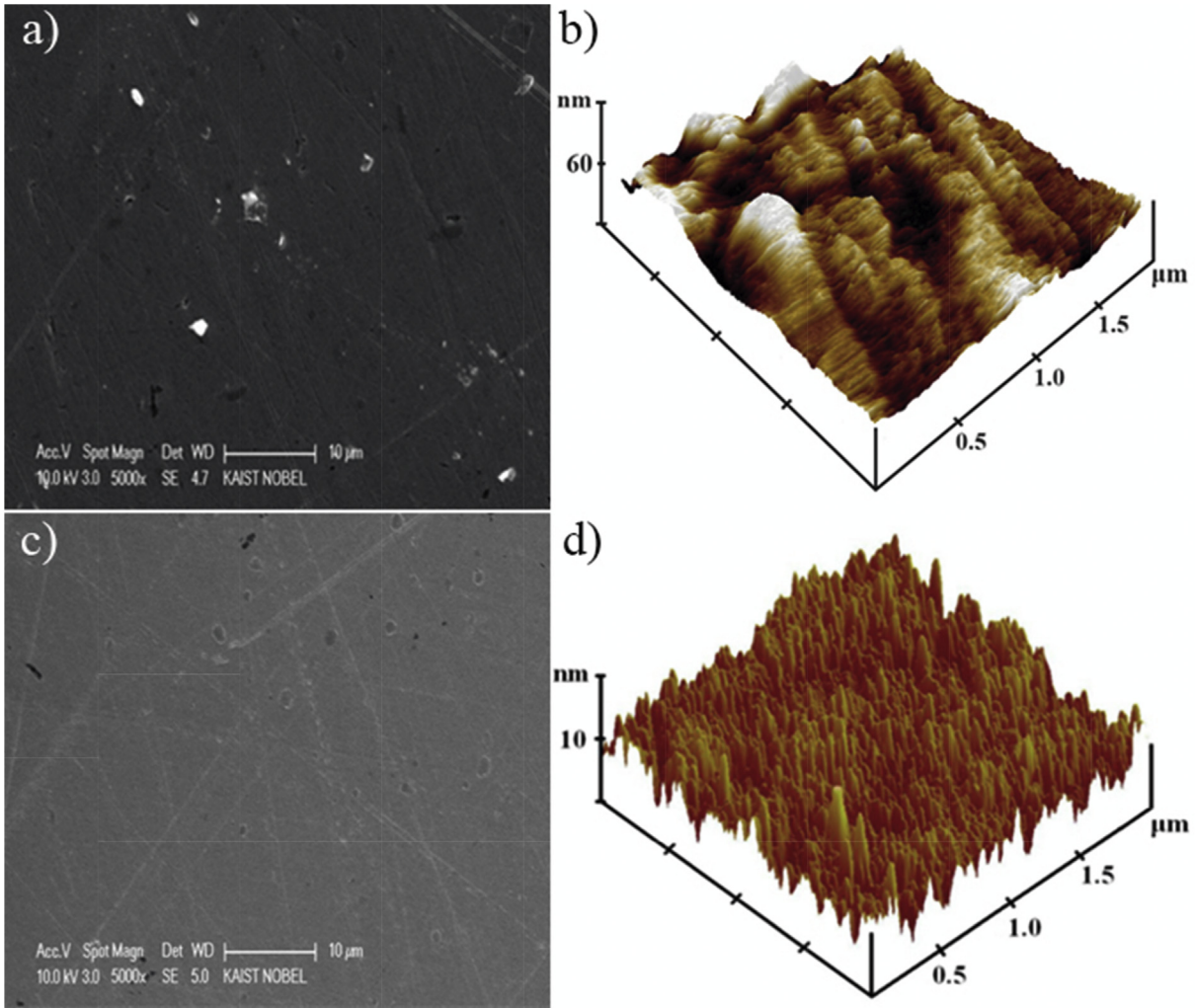


Fig. 1. Surface images of CuCrZr samples measured by SEM (left) and AFM (right) before (a), (b), and after (c), (d) mechanical polishing, respectively.

10 nm after the polishing.

The depth profiles of Auger electron spectroscopy (AES) measured from polished samples revealed that an oxygen layer, approximately 2 nm thick, exists, and average chemical compositions of the surface of the sample are 96.68, 0.41, 0.87, and 2.04 at. % for Cu, Cr, Zr and O, respectively (see Fig. 2). The existence of oxygen on the sample was not avoidable, but the oxygen layer on the surface can be removed through a plasma etching of Ar [22].

Before the loading, the full loading time of deuterium in the specimen was estimated from the following relationship [27,28]:

$$t_{lag} = d^2 / 6D \quad (1)$$

where  $t_{lag}$ ,  $d$ , and  $D$ , are lag-time, thickness of sample, and diffusivity, respectively. The values for the samples having different thicknesses at various temperatures were estimated using the transport parameters reported by Noh et al. [22], and are summarized in Table 2.

The XRD patterns measured from the polished samples revealed that the sample is an FCC structure with a lattice constant of 3.62 Å. After deuterium exposure under 25 bar at 350 °C for 24 h, there was no change in structure, and the lattice constant value with formation of an impurity phase was found within the limit of XRD resolution (see Fig. 3).

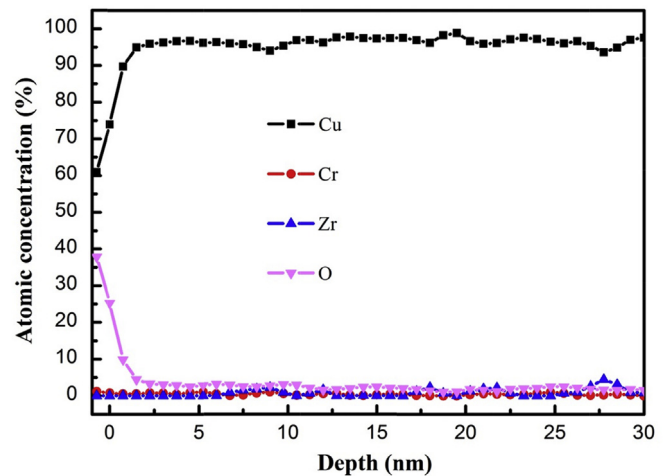
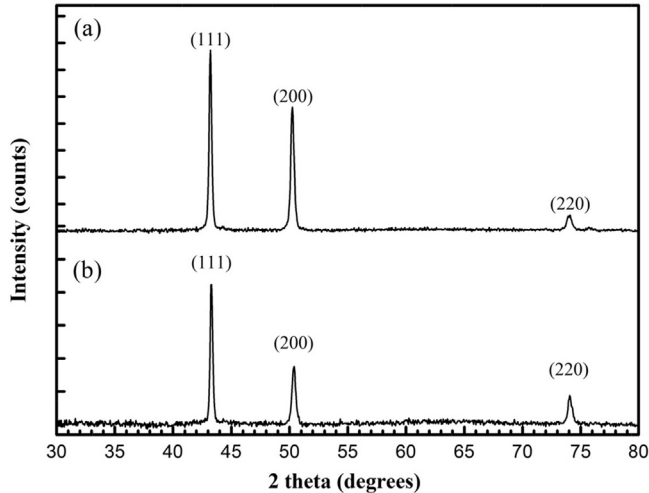


Fig. 2. Results of depth profile of AES for mechanically polished CuCrZr-ELBRODUR® G alloys.

To investigate the penetration depth of deuterium into the samples, depth profiles of secondary ion mass spectroscopy (SIMS) data were measured using Cs<sup>+</sup> primary ions with impact energy of

**Table 2**  
Deuterium loading time for CuCrZr. Diffusivity values of deuterium in the sample at various temperatures were obtained from Ref. [22].

Loading temp. (°C)	Thickness (mm)	Diffusivity ( $\text{m}^2 \cdot \text{s}^{-1}$ )	$t_{\text{lag}}$ (hours)	Full loading time (days)
120	5	$2.23 \times 10^{-16}$	829,980	93,372
240	1	$1.89 \times 10^{-13}$	61.1	6.9
240	3	$1.89 \times 10^{-13}$	550.2	61.9
240	5	$1.89 \times 10^{-13}$	978.1	110.0
350	5	$9.35 \times 10^{-12}$	19.8	2.2



**Fig. 3.** XRD patterns of CuCrZr samples measured before and after exposing 25 bar of deuterium at 350 °C for 24 h. No structural change was noted. The different intensities for (220) peaks are due to the texture effect of the samples.

15 keV in an area of  $5 \times 5 \mu\text{m}^2$  under  $6.87 \times 10^{-10}$  Torr in an analysis chamber. The distribution of embedded hydrogen and deuterium was very close and their depths were less than  $15 \mu\text{m}$  (see Fig. 4). For example, in the 240 °C loaded 5 mm thick sample, deuterium is found with a linearly decreasing intensity in a logarithmic scale down to  $10 \mu\text{m}$  from the surface, and then is rapidly diminished thereafter. One can notice in Fig. 4 that the deuterium and hydrogen concentration is also closely related to the zirconium concentration, which hints towards hydrogen isotopes possibly being trapped by zirconium atoms. The penetration depth of deuterium in CuCrZr alloy was much less than in stainless steel, which was in an order of a few tens of micrometers [29]. It should also be noted that the intensity of the elements in Fig. 4 was a relative estimation of ionized ones, and thus quantitative amounts of the elements would be calibrated by using a standard sample.

The deuterium exposed samples were baked in a vacuum to investigate the desorption behavior of deuterium depending on the thickness of the material. Fig. 5 shows the partial pressure and desorption rate of deuterium per unit area from the samples loaded at 240 °C and baked at 800 °C. The thinner samples showed a lower desorption-start temperature with a faster completion of desorption than the thicker ones. For example, in a 1 mm thick sample desorption started as low as 550 °C and lasted for 155 s, while a 5 mm thick sample shows a delayed desorption time of 320 s (Fig. 5(a)). In general, the desorption-start temperature was proportional to the thickness of the sample because the real temperature of the sample had a lag compared to the target temperature due to the heating rate being faster than the heat conductivity.

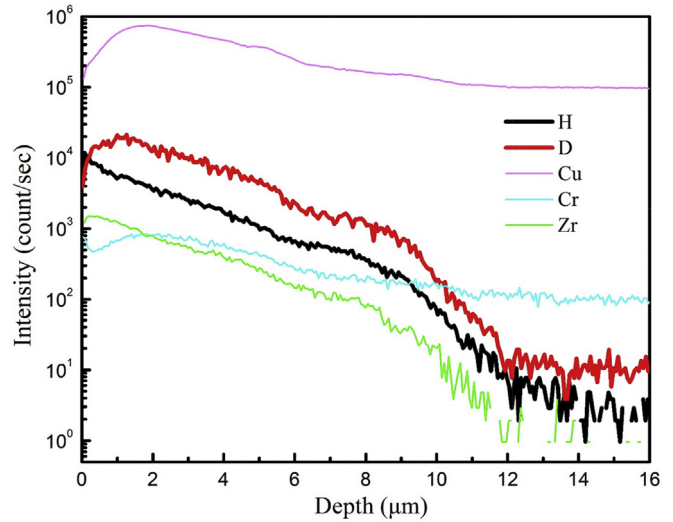


**Fig. 4.** Depth profile result of SIMS analyzed from a 5 mm thick sample exposed to deuterium at 240 °C for 24 h.

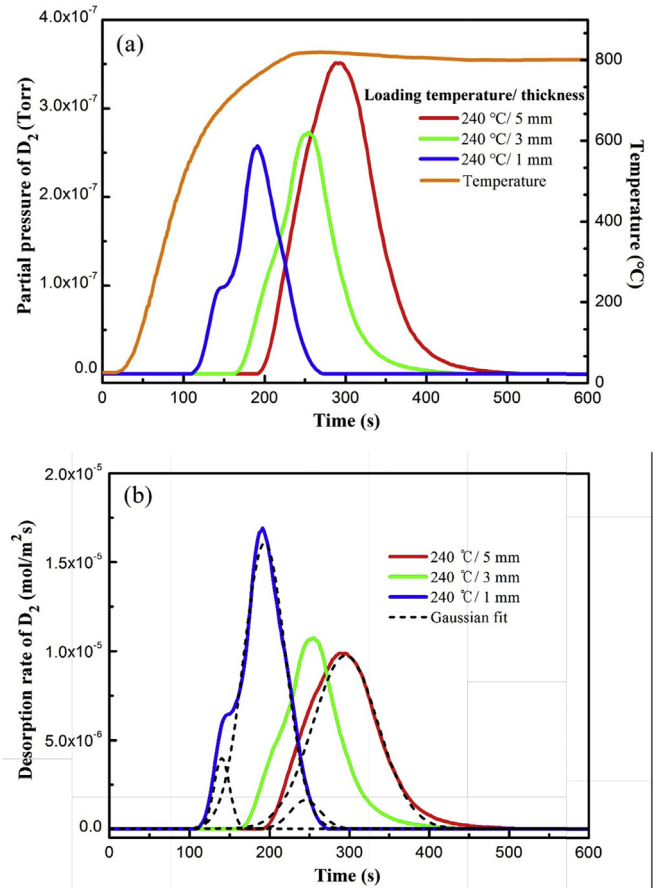


**Fig. 5.** Plots of partial pressure of deuterium (a), and desorption rates per unit area depending on sample thickness of 1, 3, 5 mm deuterated at 240 °C (b). The measured sample temperature is shown with an orange-colored line in (a), and the results of Gaussian fits for 1 and 5 mm thick samples are shown with dotted lines in (b). (For interpretation of the references to colour in this figure legend, the reader is referred to the web version of this article.)

The desorption rate of deuterium per unit area was calculated using the following formula:

$$\text{Desorption rate, } \frac{\text{mol}}{\text{m}^2\text{s}} = \frac{PP \times PS}{R \times RT \times SA} \quad (2)$$

where *PP*: partial pressure of D<sub>2</sub>, *PS*: pumping speed of the baking system which is 92.6 l/sec, *RT*: room temperature, *SA*: surface area, and *R*: gas constant. As shown in Fig. 5(b), the thinner ones show a faster desorption rate per unit area than the thicker ones because the desorption rate is inversely proportional to surface area (Eq. (2)), while none of our samples was fully deuterated. It should be noted that the peaks can be separated into two peaks (shown with dotted-lines in Fig. 5(b)) by using a Gaussian fit, suggesting that the deuterium residing on the surface desorbed first and the ones embedded in the bulk follow. For example, a 1 mm thick sample exhibits two peaks located at 130 and 180 s, and a 5 mm thick one has peaks at 245 and 295 s, which represents the desorption from near the surface and the bulk of the sample, respectively.

Fig. 6(a) shows the partial pressure of deuterium measured from the samples having the same dimension but loaded at different temperatures; 120, 240 and 350 °C. As expected, we observe in Table 2 that the samples loaded at 350 °C desorbed more deuterium than the ones deuterated at a lower temperature, which demonstrates that the absorbed amount is proportional to the loading temperature. It is interesting to note that samples loaded at 120 °C exhibited a desorption peak starting at 155 s, corresponding to 700 °C, demonstrating that deuterium absorption can take place as low as 120 °C. The total amounts of desorbed deuterium from the samples were estimated by integrating the desorption peaks, and the results of these are shown in Fig. 6 (b). For example, the 5 mm

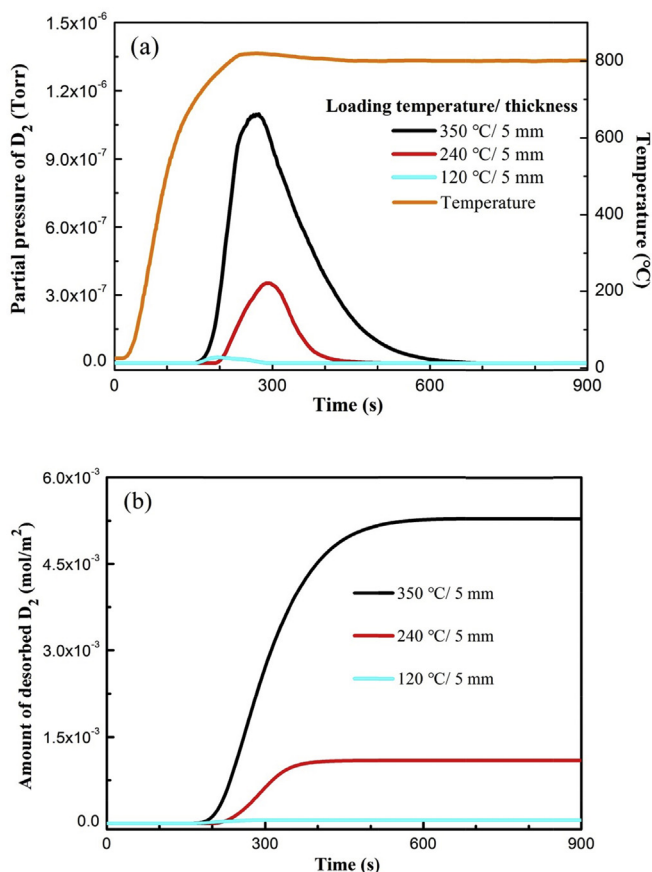


Fig. 6. Plots of partial pressure of deuterium (a), and amount of desorbed deuterium per unit area depending on loading temperature measured from 5 mm thick samples deuterated at 120, 240, 350 °C (b).

thick sample loaded at 350 °C desorbed a total of  $5.3 \times 10^{-3}$  mol/m<sup>2</sup> of deuterium.

In order to determine the parameters for optimum baking, samples were deuterated at the same condition but heated at different temperatures. Fig. 7(a) shows the partial pressure of deuterium measured from the samples deuterated at 240 °C and baked at 400, 600, and 800 °C with heating rates of 3.9, 4.2, and 3.5 °C/sec, respectively. For the samples baked at 800 °C, desorption started at 190 s corresponding to 750 °C and completed within 325 s. It should be noted that a hint of deuterium desorption was observed when baking at 400 °C, although not all of the absorbed deuterium atoms were desorbed. The significantly delayed desorption-start time for the 400 °C baked sample was due to the slow diffusion of deuterium to the sample. Baking at a higher temperature resulted in a faster completion of desorption than desorbing at a lower temperature. When the samples were baked at 600 °C, no further desorption was noted after 700 s. The fact that the desorbed amount of deuterium from the sample baked at 600 °C exceeded the amount extracted when baking at 800 °C can be explained through the statistical difference between two samples (~35%). The total amount of desorbed deuterium was also estimated by integrating the desorption peaks, and the results are shown in Fig. 7(b).

To check whether or not the desorption was completed when baking at 800 °C, samples were placed at 800 °C in a dynamic vacuum for 20 min and after confirming that there was no further

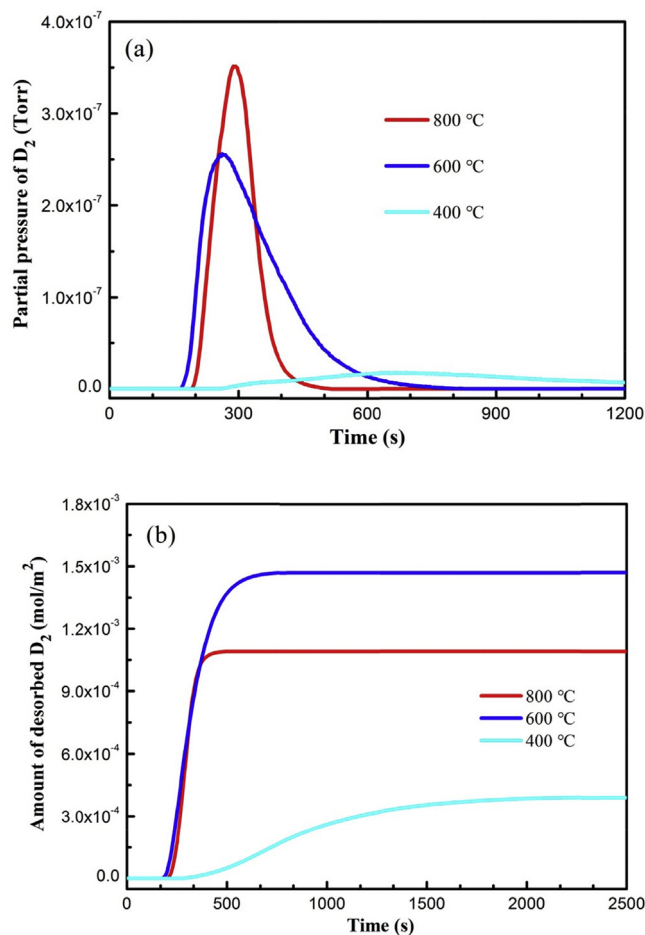
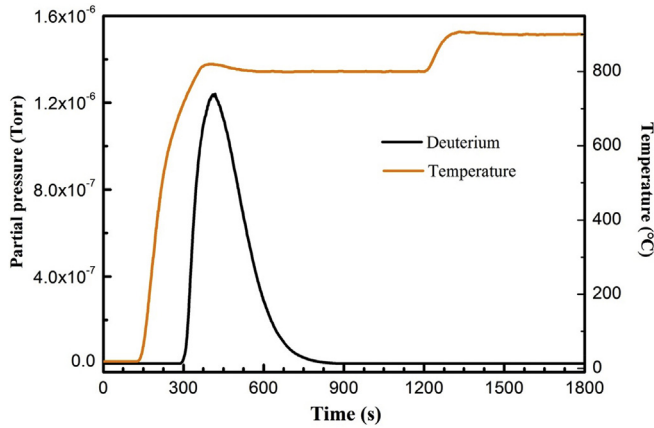


Fig. 7. Plots of deuterium partial pressure (a), and amount of desorbed deuterium depending on baking temperature measured from 5 mm thick samples deuterated at 240 °C (b).



**Fig. 8.** Plot of partial pressure for deuterium measured from 5 mm thick sample deuterated at 350 °C for 24 h and baked at 800 and 900 °C. The measured sample temperature is shown with an orange-colored line. (For interpretation of the references to colour in this figure legend, the reader is referred to the web version of this article.)

desorption, the temperature was increased to 900 °C. As shown in Fig. 8, the appearance of a prominent deuterium peak during the heating to 800 °C with no hint of further desorption at 900 °C demonstrates that 800 °C is an efficient condition for the complete removal of the embedded deuterium in CuCrZr alloys.

To calculate the trapping energy for deuterium, 5 mm thick samples deuterated at 350 °C were heated using the TDS system at heating rates from 10 to 30 °C/min, followed by the heating parameters proposed by Poon et al. [11], and the results of partial pressure for deuterium as a function of temperature are shown in Fig. 9(a). The samples heated at 10, 15, 20, 30 °C/min apparently exhibited one broad, but with a hint of a shoulder, desorption peak starting at 405, 428, 488 and 528 °C. All peaks can be split into two distinct peaks by using a Gaussian fit, which suggests two sites for the trapping energy. Based on the results of the fits shown with dotted-lines in Fig. 9(a), the desorption energy,  $E_d$ , which is same as the activation energy for deuterium needed to escape from the trapping site, is obtained from the relation between the temperature of the desorption peak maximum,  $T_c$ , and the heating rate  $\Phi$  [30]:

$$\frac{E_d \Phi}{RT_c^2} = A \cdot \exp\left(-E_d/RT_c\right) \quad (3)$$

where  $R$  is the gas constant. This classical equation was modified in terms of heating rate and temperature for the maximum desorption:

$$\frac{d \ln(\Phi/T_c^2)}{d T_c^{-1}} = -\frac{E_d}{R} \quad (4)$$

The desorption energy was calculated from the linear fit to the differentials of  $\ln(\Phi/T_c^2)$  and  $T_c^{-1}$  for the four Gaussian fitted peaks with different heating rates, and the results are shown in Fig. 9(b). Accepting the two assumptions that 1) the distribution of available sites for deuterium in the sample obeys the Gaussian function, and 2) an occupation of deuterium follows the Fermi-Dirac statistics because one deuterium occupies one site, we estimate the trapping energies of 62 and 79 kJ/mol, which is very close to the trapping energies of hydrogen in Cu measured by Takagi [27], and is in the range of the values measured from hydrogen in Fe and Al having different trapping sites such as

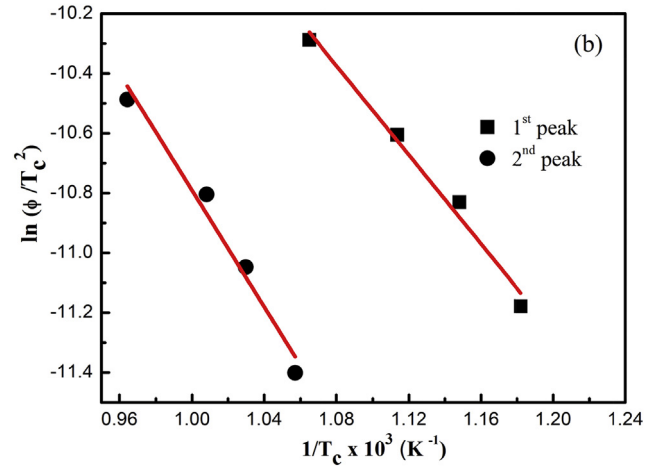
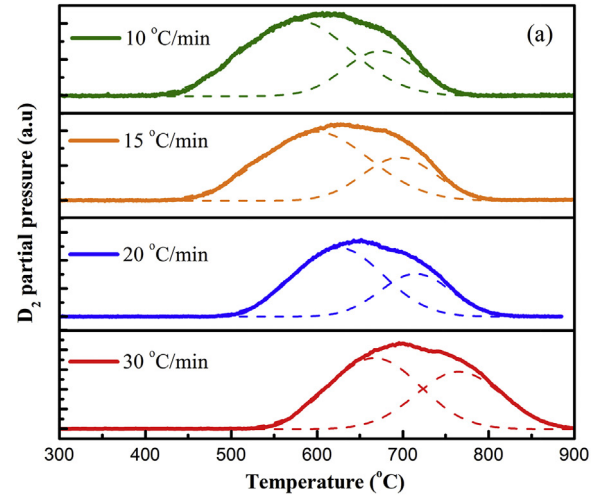


**Fig. 9.** (a) TDS results for deuterium loaded samples desorbed with different heating rates from 10 to 30 °C/min, and (b) plot of relationship between  $\ln(\Phi/T_c^2)$  and  $T_c^{-1}$ . The Gaussian fits for the desorption peaks are shown with dotted-lines in (a).

grain boundary, vacancy, dislocation and interstitials [30,31].

#### 4. Conclusion

To evaluate the engineering applications of CuCrZr alloys for plasma structural materials in fusion reactors, desorption dynamics of deuterium in the materials as functions of sample thickness, loading and baking temperatures were investigated following the ITER scope. After exposing the sample to 25 bar of deuterium at 350 °C for 24 h, no change in the structure or the lattice constant was noted, while RGA detected a significant amount of deuterium during the baking of the sample as low as 400 °C. Depth profiles of SIMS results showed that deuterium diffuses into the sample to a depth of 15  $\mu\text{m}$  and can be completely retrieved in 15 min by heating in a vacuum at 800 °C. The amounts of desorbed deuterium were estimated by integrating the desorption peak of RGA, and the value, for example, was  $5.3 \times 10^{-3} \text{ mol/m}^2$  for the 5 mm thick sample deuterated at 350 °C. For the samples having the same dimension, the amount of desorbed deuterium was proportional to the loading temperature. We noted that the CuCrZr alloy absorbs deuterium as low as at 120 °C and desorbs it at 400 °C, although the

complete retrieval of deuterium can be obtained at 800 °C using a dynamic pumping in 15 min. The trapping energy for deuterium was calculated by analyzing TDS data heated at different heating rates from 10 to 30 °C/min. By employing an Arrhenius plot and Fermi-Dirac statistics following the Gaussian distribution function, we estimated the trapping energies to be 62 and 79 kJ/mol, which are mainly attributed to the interstitials in the alloy.

### Acknowledgements

This research was supported by Basic Science Research Program through the National Research Foundation of Korea (NRF) funded by the Ministry of Education, Science and Technology (NRF-2015M1A7A1A01002238, 2016K1A4A3914691).

### References

- [1] M. Lipa, A. Durocher, R. Tivey, T. Huber, B. Schedler, J. Weigert, The use of copper alloy CuCrZr as a structural material for actively cooled plasma facing and in vessel components, *Fusion Eng. Des.* 75 (2005) 469–473.
- [2] L. Doceul, J. Bucalossi, S. Larroque, M. Lipa, C. Portafaix, A. Saille, F. Samaille, B. Soler, F. Ferlay, J. Verger, Design, integration and feasibility studies of the Tore-Supra West divertor structure, *Fusion Eng. Des.* 88 (2013) 814–817.
- [3] A.L. Puma, L. Giancarli, Y. Poitevin, J.-F. Salavy, P. Sardain, J. Szczepanski, Optimization of a water-cooled divertor for the European power plant conceptual study, *Fusion Eng. Des.* 61 (2002) 177–183.
- [4] M. Hatakeyama, H. Watanabe, M. Akiba, N. Yoshida, Low void swelling in dispersion strengthened copper alloys under single-ion irradiation, *J. Nucl. Mater.* 307 (2002) 444–449.
- [5] A. Pokrovsky, S. Fabritsiev, D. Edwards, S. Zinkle, A. Rowcliffe, Effect of neutron dose and irradiation temperature on the mechanical properties and structure of dispersion strengthened copper alloys, *J. Nucl. Mater.* 283 (2000) 404–408.
- [6] G. Kalinin, V. Barabash, A. Cardella, J. Dietz, K. Ioki, R. Matera, R. Santoro, R. Tivey, T.I.H. Teams, Assessment and selection of materials for ITER in-vessel components, *J. Nucl. Mater.* 283 (2000) 10–19.
- [7] S. Fabritsiev, A. Pokrovsky, A. Peacock, M. Roedig, J. Linke, A. Gervash, V. Barabash, Effect of irradiation temperature and dose on mechanical properties and fracture characteristics of Cu/SS joints for ITER, *J. Nucl. Mater.* 386 (2009) 824–829.
- [8] V. Barabash, G. Kalinin, S.A. Fabritsiev, S.J. Zinkle, Specification of CuCrZr alloy properties after various thermo-mechanical treatments and design allowables including neutron irradiation effects, *J. Nucl. Mater.* 417 (2011) 904–907.
- [9] J.-H. You, A. Brendel, S. Nawka, T. Schubert, B. Kieback, Thermal and mechanical properties of infiltrated W/CuCrZr composite materials for functionally graded heat sink application, *J. Nucl. Mater.* 438 (2013) 1–6.
- [10] E. Bloom, D. Smith, Structural materials for fusion reactor blanket systems, *J. Mater. Energy Syst.* 7 (1985) 181–192.
- [11] M. Poon, A. Haasz, J. Davis, Modelling deuterium release during thermal desorption of D<sup>+</sup>-irradiated tungsten, *J. Nucl. Mater.* 374 (2008) 390–402.
- [12] S. Lee, H. Kim, B.-H. Chung, S. Noh, Study of an experimental system for hydrogen permeation in thin-solid materials for fusion plasma research, *Curr. Appl. Phys.* 11 (2011) S99–S102.
- [13] K. Sugiyama, C. Porosnicu, W. Jacob, I. Jepu, C. Lungu, Investigation of deuterium retention in/desorption from beryllium-containing mixed layers, *Nucl. Mater. Ener.* 6 (2016) 1–9.
- [14] S. Lee, S.-H. Yun, H.G. Joo, S. Noh, Deuterium transport and isotope effects in type 316L stainless steel at high temperatures for nuclear fusion and nuclear hydrogen technology applications, *Curr. Appl. Phys.* 14 (2014) 1385–1388.
- [15] S. Noh, S. Lee, H. Kim, S.-H. Yun, H.G. Joo, Deuterium permeation and isotope effects in nickel in an elevated temperature range of 450–850 °C, *Int. J. Hydrogen Energy* 39 (2014) 12789–12794.
- [16] S. Noh, S. Lee, W. Byeon, Y. Chun, Y. Jeong, Transport of hydrogen and deuterium in the reduced activation martensitic steel ARAA, *Fusion Eng. Des.* 89 (2014) 2726–2731.
- [17] S. Steward, Review of Hydrogen Isotope Permeability through Materials, Lawrence Livermore National Lab, CA (USA), 1983.
- [18] C. San Marchi, B.P. Somerday, Technical Reference on Hydrogen Compatibility of Materials, SAND2008–1163, Sandia National Laboratories, Livermore CA, 2008.
- [19] J. Zhao, Q. Wang, D. Liu, Z. Wang, K. Fang, T. Wang, J. Kasagi, Dynamical concentration and static retention of deuterium in tungsten foil studied by low energy D (d,p) T reaction and elastic recoil detection, *Nucl. Instrum. Method Phys. Res. B* 360 (2015) 139–144.
- [20] R. Anderl, M. Hankins, G. Longhurst, R. Pawelko, Deuterium transport in Cu, CuCrZr, and Cu/Be, *J. Nucl. Mater.* 266 (1999) 761–765.
- [21] E. Serra, A. Perujo, Hydrogen and deuterium transport and inventory parameters in a Cu–0.65 Cr–0.08 Zr alloy for fusion reactor applications, *J. Nucl. Mater.* 258 (1998) 1028–1032.
- [22] S. Noh, W. Byeon, H. Shin, H. Kim, J. Kim, S. Lee, J. Kim, Hydrogen-isotope transport in an ELBRODUR G CuCrZr alloy for nuclear applications in heat sinks, *J. Nucl. Mater.* 473 (2016) 112–118.
- [23] G. Young, J. Scully, The diffusion and trapping of hydrogen in high purity aluminum, *Acta Mater.* 46 (1998) 6337–6349.
- [24] S.-i. Hayashi, Measurement of hydrogen diffusivity in aluminum and a dilute alloy by thermal evolution spectroscopy, *Jpn. J. Appl. Phys.* 37 (1998) 930.
- [25] S.W. Smith, J.R. Scully, The identification of hydrogen trapping states in an Al-Li-Cu-Zr alloy using thermal desorption spectroscopy, *Metall. Trans. A* 31 (2000) 179–193.
- [26] I. Takagi, M. Akiyoshi, N. Matsubara, T. Nishiuchi, K. Moritani, T. Sasaki, H. Moriyama, Characteristics of traps for hydrogen in helium-irradiated copper, *J. Nucl. Mater.* 367 (2007) 489–493.
- [27] I. Peñalva, B. Riccardi, F. Legarda, G. Esteban, G. Alberro, Interaction of Copper Alloys with Hydrogen, INTECH Open Access Publisher, 2012.
- [28] F. Reiter, K. Forcey, G. Gervasini, A Compilation of Tritium-material Interaction Parameters in Fusion Reactor Materials, ECSC-EEC-EAEC, Brussels–Luxemburg, 1993. Catalog number: CD-NA-15217-EN-C.
- [29] R. Calder, T. Elleman, K. Verghese, Grain boundary diffusion of tritium in 304- and 316-stainless steels, *J. Nucl. Mater.* 46 (1973) 46–52.
- [30] W. Choo, J.Y. Lee, Thermal analysis of trapped hydrogen in pure iron, *Metall. Trans. A* 13 (1982) 135–140.
- [31] T. Izumi, G. Itoh, Thermal desorption spectroscopy study on the hydrogen trapping states in a pure aluminum, *Mat. Trans.* 52 (2011) 130–134.